LAWRENCE
LIVERMORE
NATIONAL
LABORATORY

LLNL-CONF-686221

Revisiting Fenton Hill Phase I reservoir creation and stimulation mechanisms through the GTO code comparison effort

P. Fu, M. W. McClure, S. Shiozawa, M. D. White

March 17, 2016

50th US Rock Mechanics/Geomechanics Symposium
Houston, TX, United States
June 26, 2016 through June 29, 2016

Disclaimer

This document was prepared as an account of work sponsored by an agency of the United States government. Neither the United States government nor Lawrence Livermore National Security, LLC, nor any of their employees makes any warranty, expressed or implied, or assumes any legal liability or responsibility for the accuracy, completeness, or usefulness of any information, apparatus, product, or process disclosed, or represents that its use would not infringe privately owned rights. Reference herein to any specific commercial product, process, or service by trade name, trademark, manufacturer, or otherwise does not necessarily constitute or imply its endorsement, recommendation, or favoring by the United States government or Lawrence Livermore National Security, LLC. The views and opinions of authors expressed herein do not necessarily state or reflect those of the United States government or Lawrence Livermore National Security, LLC, and shall not be used for advertising or product endorsement purposes.

ARMA 16-0841

Revisiting Fenton Hill Phase I reservoir creation and stimulation mechanisms through the GTO code comparison effort

Fu, P.
Lawrence Livermore National Laboratory, Livermore, CA, USA
McClure, M.W.
McClure Geomechanics LLC, Palo Alto, CA, USA
Shiozawa S.
University of Texas, Austin, TX, USA
White, M.D.
Pacific Northwest National Laboratory, Richland, WA, USA

This paper was prepared for presentation at the 50th US Rock Mechanics / Geomechanics Symposium held in Houston, Texas, USA, 26-29 June 2016. This paper was selected for presentation at the symposium by an ARMA Technical Program Committee based on a technical and critical review of the paper by a minimum of two technical reviewers. The material, as presented, does not necessarily reflect any position of ARMA, its

ABSTRACT: A series of experiments performed at the Fenton Hill hot dry rock site after stage 2 drilling of Phase I reservoir provided intriguing field observations on the reservoir's responses to injection and venting under various conditions. Two teams participating in the US DOE Geothermal Technologies Office (GTO)'s Code Comparison Study (CCS) used different numerical codes to model these five experiments with the objective of inferring the hydraulic stimulation mechanism involved. The codes used by the two teams are based on different numerical principles, and the assumptions made were also different, due to intrinsic limitations in the codes and the modelers' personal interpretations of the field observations. Both sets of models were able to produce the most important field observations and both found that it was the combination of the vertical gradient of the fracture opening pressure, injection volume, and the use/absence of proppant that yielded the different outcomes of the five experiments.

1. INTRODUCTION

Two decades after the conclusion of the Fenton Hill Hot Dry Rock (HDR) project, disagreements still exist among experts regarding the reservoir creation and stimulation mechanisms in the two phases of the field experiments. The emergence and continued improvement of more advanced computer simulation codes for geothermal applications in recent years provide new opportunities for evaluating competing hypotheses against the rich set of observations and measurements at Fenton Hill, and promise a better understanding of the enhanced geothermal reservoirs created. The US Department of Energy (DOE) Geothermal Technologies Office (GTO) is sponsoring a code comparison study (CCS), organized and executed by Pacific Northwest National Laboratory (PNNL), aiming at testing, diagnosing differences, and demonstrating modeling capabilities of a worldwide collection of numerical simulators for evaluating geothermal technologies (White et al. 2015; White et al. 2016). The GTO CCS is currently in the "challenge problem" phase, which focuses on modeling a variety of field data and observations in the Fenton Hill HDR project. This paper presents the preliminary results of two participating teams on one of the challenge problems.

2. PROBLEM STATEMENT

This paper tackles Part I (reservoir creation and stimulation) of Challenge Problem #2 in the GTO CCS. The problem concerns a series of pressurization and venting experiments in Zone 7 of well GT-2 after stage 2 drilling of Fenton Hill Phase I, performed in September 1974. These experiments provided intriguing field observations that make it possible to infer the hydraulic stimulation mechanism involved. Zone 7 is the open-hole interval at the bottom of well GT-2 after stage 2 drilling (2043 m deep). Field observations indicated that two natural joints between 1990-1993 m and 1999-200 m deep, respectively, approximately dipping 70 degrees, might have been opened by the stimulation. Key observations in the five injection, shut-in and subsequent venting experiments included:

1) Pressure limiting behavior: injection rate rapidly increased once the wellhead pressure reaches 17.2 MPa (2500 psi);

2) Shut-in pressure declined after the first injection exercises, as depicted in Figure 3-9 of Brown et al. (2012);

3) The small flow-back ratio of the injected water in the first four water injection experiments; and

4) The very high fluid recovery rate after the fifth injection, which used cross-linked gel mixed with sand.

Each participating team is asked to simulate these injection, shut-in, and flow back operations, using assumptions consistent with conditions reported in Brown et al. (2012) and other Fenton Hill related publication, with the objective of reproducing these field observations and offering insight into the associated stimulation mechanisms. This paper presents the preliminary results from two of the participating teams, Team A and Team B, who have used codes based on very different numerical methods.

Note that the design of this challenge problem heavily relied on information provided in Section *Stage 2 Pressure-Stimulation Tests* of Chapter 3 in Brown et al. (2012). More detailed descriptions of the GTO CCS's two challenge problems are available in White et al. (2016).

3. COMMON ASSUMPTIONS AND CONSIDERATIONS OF BOTH TEAMS

The results reported herein by both teams assume the stimulations involved the opening of a pre-existing fracture or pre-existing fractures.

There is uncertainty about the state of stress. Kelkar et al. (1986) proposed that the minimum principal stress gradient is 19 MPa/km (38 MPa at the injection depth). However, Brown (1989) proposed that the minimum principal stress gradient is 13 MPa/km (26 MPa at the injection depth). Barton and Zoback (1988) used wellbore breakouts to estimate that the minimum principal stress is oriented at 60°W of N and that the vertical and maximum horizontal stresses have similar magnitude. In the injection/pressure data, injection pressure becomes nearly insensitive to injection rate at a pressure around 17.2 MPa (bottomhole pressure around 37 MPa), an indication that fracture opening occurred when the fluid pressure reached the fracture normal stress. According to the Kelkar stress profile, the bottomhole pressure is close to the minimum principal stress, which implies that either a hydraulic fracture formed at the well or that the injection opened a natural fracture oriented perpendicular to the minimum principal stress. According to the Brown (1989) profile, the bottomhole pressure significantly exceeded the minimum principal stress. In this scenario, the fracture opening pressure represents the normal stress on natural fractures inclined from the direction perpendicular to the minimum principal stress. Brown et al. (2012) report that spinner logs run during injection indicated two discrete zones of fluid acceptance, supporting the theory that preexisting fractures took the fluid, rather than axial hydraulic fractures. For the purposes of this exercise, only the normal stress acting on the existing fracture plane, which is approximately the fracture opening pressure, affects the results. Both scenarios predict that the natural fracture(s) connected to the wellbore has an opening pressure of 37 MPa. The difference between the two scenarios, regarding whether the existing fracture is perpendicular to or oblique to the minimum principal stress direction, will affect the potential creation of splay fractures off the existing fracture(s). Also, proppant transport could be affected if fluid is injected primarily into inclined, rather than vertical, fractures. The potential effects of these processes are not investigated in the present results.

The five injection tests are idealized with the following schedule: (1) Test 1, 8 l/s for 60 s, followed by one hour of shut-in, (2) Test 2, 10.6 l/s for 3928 s, (3) Test 3, 10.6 l/s for 7141 s, (4) Test 4, 10.6 l/s for 12,858 s, and (5) Test 5, 23.9 l/s for 713 s with proppant concentration of 253 kg proppant per m^3 of slurry. Test 1 has a one-hour shut-in following the injections, and then venting (flow back). We assume Tests 2 to 4 to each have a five-minute shut-in period between injection and venting for. In the simulation of Test 5, venting/flow-back immediately follows injection, mimicking the field operation as documented in Brown et al. (2012).The other four tests each have venting immediately or soon after injection.

We assume the natural fracture to have been saturated with water at hydrostatic *in situ* pressure (~19.6 MPa at 2000 deep). Brown (1989) suggested the far-field pore pressure at the Fenton Hill site to be 5.4 MPa below hydrostatic. Team B's simulation found that this condition would cause the Test 1 shut-in pressure (wellhead) to decline along a pattern different from what was observed. Since Brown's estimation applies to the site as a whole, it does not necessarily contradict our hydrostatic assumption at this specific depth. The shear modulus of the rock is assumed to be 15 GPa and Poisson's ratio is assumed to be 0.25.

A complication in the interpretation of Test 5 (gel injection with proppant), as discovered by Team A, is that it is uncertain whether proppant actually entered the formation. Based on Figure 3-8 from Brown et al. (2012), the wellbore volume was around 21-25 m^3. However, during the proppant injection period, 17 m^3 of fluid were injected. Proppant would not enter the formation until fully displacing the fluid already in the wellbore. Brown (personal communication) reports that proppant was believed to have entered the formation because the injection pressure sharply increased by several 10s of psi a few minutes before shut-in. One possibility is that because the proppant is denser than water, it settled downward through the well faster than the fluid being pumped. It is also possible that proppant did not actually enter the formation and some other process was responsible for the pressure increase that was interpreted as proppant entering the formation. The

two teams used different assumptions to handle the effects of the proppant, as described below.

4. SIMULATION OF TEAM A

4.1. The Numerical Model

Team A uses the 3D version of CFRAC (Complex Fracturing ReseArch Code), which can perform simulations of proppant transport, including gravitational settling, screen-out, and fracture closure (Shiozawa and McClure, 2016). CFRAC is a discrete fracture network simulator that fully couples single-phase flow with the stresses induced by fracture opening and sliding. For proppant simulation, the code includes a simple wellbore model to track the transport of proppant from the surface to the formation.

When the effective normal stress on a fracture is compressive, the fracture is considered mechanically closed. For closed fractures, the code uses a Barton-Bandis (Barton et al. 1985) joint closure law to describe the relationship between fracture aperture and effective normal stress. When the effective normal stress on a fracture element becomes tensile, the element mechanically opens. The simulator calculates the opening displacement of all fracture elements simultaneously, while enforcing the stress equilibrium condition that the effective normal stress of an open fracture must be equal to zero (Crouch and Starfield, 1983). The fractures are meshed into elements, allowing parts of the fracture to be mechanically opened and others to be mechanically closed. The stresses induced by fracture deformation are calculated using the boundary element method of Okada (1992), which assumes small-strain, that the formation is homogeneous and linearly elastic, and that the fractures are embedded in an infinite half-space. The cubic law is used to relate fracture aperture to transmissivity. Leakoff is described using a semi-analytical one-dimensional leakoff model (Vinsome and Westerveld, 1980), which, unlike the Carter leakoff model, accounts for the changing fluid pressure in the fracture over time. The simulations are isothermal. Poroelastic stress changes due to fluid leakoff into the matrix are neglected. Non-Darcy pressure drop in the fractures is included (Fourar et al., 1993) using the method described by McClure et al. (2015).

The constitutive relations developed by Dontsov and Peirce (2014) are used to describe fluid and proppant flow in the fractures. They smoothly capture the transition between two extremes: (1) dilute proppant concentrations when fluid flow is well-described by the cubic law and proppant moves freely, and (2) very high proppant concentrations when the proppant becomes immobile and fluid flow is well-described by Darcy's law for flow through a porous medium. Gravitational settling of the proppant is included.

4.2. Model Setup

In addition to the common assumptions presented in Section 3, Team A assumed the natural fracture to be vertical, square in shape (170 m in each dimension), and intersecting the wellbore at 25 m above the bottom edge. The matrix permeability is 5 microDarcy, matrix porosity 5%, and matrix compressibility 0.00145 MPa^{-1}. The proppant density is 2500 kg/m3, and the proppant diameter is 250 microns (around 70 mesh). The value of E_0 is assumed to be 110 microns, and $\sigma_{n,ref}$ is 5 MPa (refer to Shiozawa and McClure, 2016 for description of these variables)

The five tests are modeled in a single simulation, with ten hours of flow-back between the end of the shut-in of the previous test and the beginning of the pumping of the subsequent test.

Brown et al. (2012) reports that in Test 5 a cross-linked gel was pumped with the proppant, which would be expected to have a viscosity on the order of 100 cP or more. However, this gel would thermally degrade, a process that CFRAC does not have the capability to describe. Also, as described in Section 3, it is unclear whether the gel entered the formation. For simplicity, the viscosity is set to 1 cP for the full duration of the simulation, much lower than the viscosity of the cross-linked gel, but slightly higher than the viscosity of water at reservoir conditions. Fluid viscosity affects: (1) the ability of the fluid to carry proppant through the fracture and resist gravitational settling, (2) the pressure required to inject fluid into the fracture, and (3) the rate of fluid leakoff. Because of the uncertainty and complexity regarding the fluid viscosity, this remains an important uncertainty in the overall modeling process.

Team A also assumes that proppant entered the formation several minutes before the end of injection. To accomplish this, the wellbore volume in the simulation is decreased slightly.

4.3. Results for Test 1

The main observable in Test 1 is the pressure decline curve during the one-hour shut-in period. Team B finds that the rate of pressure decline is primarily controlled by spreading of fluid within the fracture, which depends on the aperture of the natural fracture and its sensitivity to effective stress. The fluid leakoff into the matrix plays a relatively minor role. In the tuned model, the fracture aperture is 110 microns at effective normal stress equal to zero, and 11 microns at effective normal stress of 5 MPa. This means that the aperture is highly stress dependent, which causes significant pinching off near the well during flow-back. The simulated pressure

decline during the shut-in of Test 1 is shown in Fig. 1, which matches the field data fairly well. The same joint closure parameters are used in all subsequent simulations of Team A.

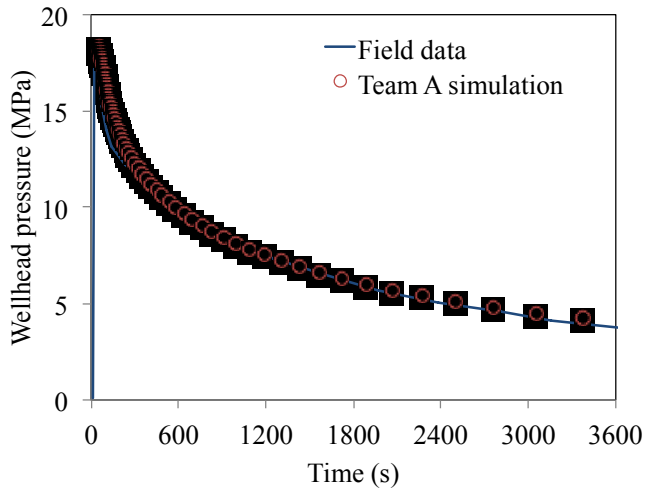

Fig. 1. Simulated Test 1 shut-in pressure decline curve by Team A.

4.4. Results for Tests 2 to 4

The fluid pressure distribution in the fracture near the end of Test 2 is shown in Fig. 2. The fluid has an apparent tendency to move upwards, likely due to the great vertical gradient of the fracture opening pressure. In other words, it takes less "hydraulic head" to open the fracture at a higher location than at a lower one, so fluid is motivated to move upward. The flow rate history in Test 2 is shown in Fig. 3. When the venting starts, there is a instantaneous peak (negative) of the flow-back, but the flow-back rate quickly diminishes due to the "pinching off" effect near the wellbore. The total fluid recovery ratio in one hour is only 1.7%, consistent with the field observation of very low ratio, although the exact value in the field was not reported in Brown et al. (2012).

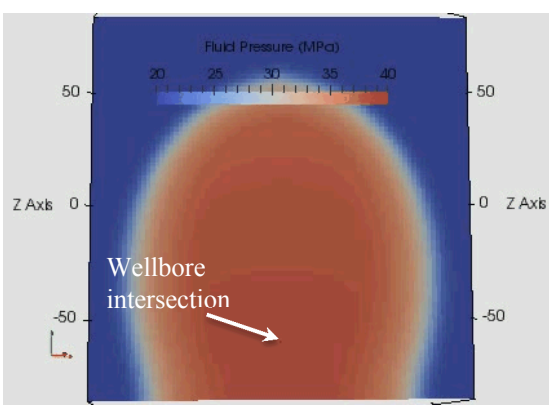

Fig. 2. Fluid pressure distribution in the fracture near the end of the injection in Test 2.

The simulated fluid recovery ratios in Test 3 and Test 4 are also shown in Table 1. The more fluid injected, the lower is the recovery ratio, as expected.

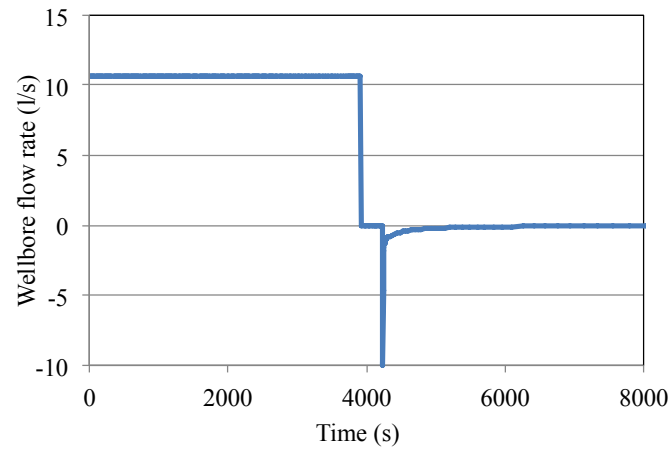

Fig. 3. Simulated wellbore flow rate for Test 2 by Team A. A positive value means injection and negative values mean flow-back.

	Injected volume (m^3)	1-hour recovery ratio	10-hour recovery ratio
Test 1	0.5	10.7%	19.7%
Test 2	42	1.7%	2.5%
Test 3	46	1.4%	2.3%
Test 4	136	1.0%	2.0%
Test 5	17	26.0%	73%
[a]Test 5 without proppant	17	12.1%	19%

Note: a Hypothetical case for investigating mechanisms.

4.5. Results for Test 5

An important feature that differentiates Test 5 from the other four tests is the use of proppant. Fig. 3 shows the simulated concentration of proppant at the end of ten hours of flow back. During injection, the proppant had been carried by the fluid to more than 20 m from the wellbore. In the venting process, the proppant effectively mitigates the pinching-off near the wellbore by holding (or "propping") open the fracture. In Fig. 5, we see that the flow-back rate is sustained for a much longer time than in Test 2 (Fig. 2). The total fluid recovery ratio reaches 73% in ten hours, according to the simulation results.

To quantify the effects of proppant, Team A performs a "control" simulation where no proppant is used whereas all the other aspects of the model remains unchanged. The recovery ratios at one hour and ten hours are 12.1% and 19%, respectively. These are substantially lower than the values from the model with proppant, but nevertheless much higher than the corresponding values from Tests 2 to 4. This is because the previous injections were longer duration and larger volume, allowing more

time for fluid to leak off into the surrounding formation as well the part of the fracture far from the injection point. Also, each injection increases the pressure surrounding the fracture, decreasing leakoff rate in subsequent injections. The results show that proppant is the main factor responsible for the very high fluid recovery ratio in Test 5. The proppant is limited to a relatively near-wellbore region due to screenout. The fracture aperture is not large enough to allow proppant to flow far from the well. In reality, thermoelastic stresses caused by the cold water injection would probably determine the size of this screenout region. If viscous gel were successfully placed in the formation, this might increase the aperture sufficiently to allow the proppant to be transported further from the well.

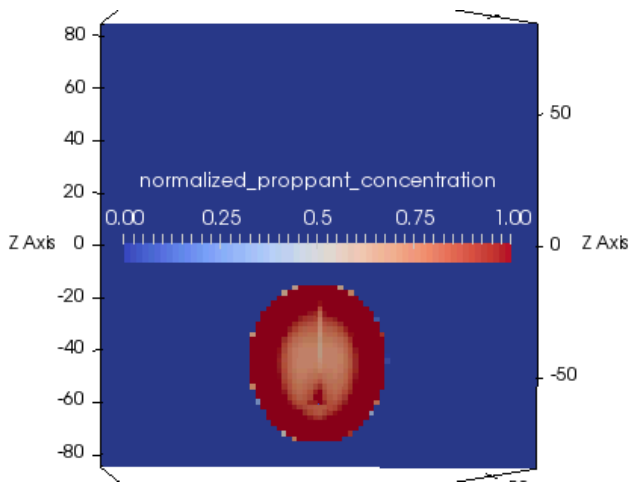

Fig. 4. Simulated proppant concentration X minutes after the injection has started.

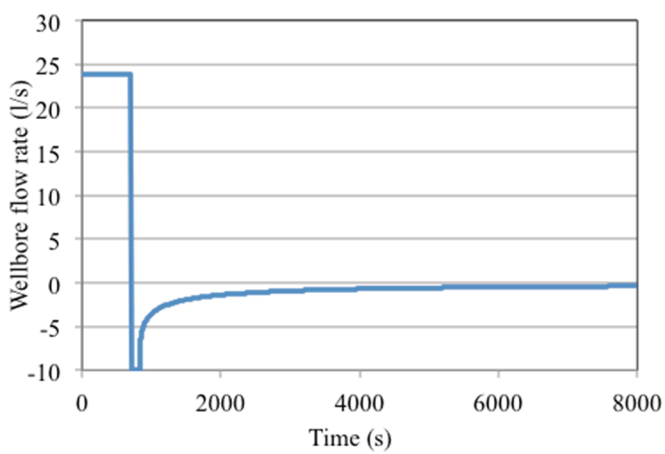

Fig. 5. Simulated wellbore flow rate for Test 5 by Team A. A positive value means injection and negative values mean flow-back.

5. SIMULATION OF TEAM B

5.1. The Numerical Model

Team B employs GEOS, a fully coupled hydraulic fracture simulation code developed at the Lawrence Livermore National Laboratory for the current study. GEOS uses the finite element method (FEM) to calculate the rock solid's stress and deformation under external loading and fracture fluid pressure. Fractures exist and propagate along a "face" mesh consisting of faces of the FEM solid elements. Parallel plate flow along the fractures, assuming the lubrication theory, is handled by the finite volume method (FVM). The solid and flow solvers are coupled together explicitly: the fluid pressure obtained by the FVM solver is applied on the solid mesh as stress boundary conditions whereas the aperture in the flow solver is based on the deformation in the FEM mesh. A stress intensity factor-based criterion is employed to handle the propagation of fractures based the principles in linear elastic fracture mechanics (LEFM). If the fluid pressure in a fracture is lower than the normal stress acting on the fracture, the fracture is "closed" and a contact model with Coulomb's friction law is invoked to handle it. Fu et al. (2013) described in detail the aforementioned modeling approach in an early 2D version of GEOS; the current 3D version is considerably more complex (Settgast et al. 2016), but the basic principles remain the same.

5.2. Model Setup

The Team B model makes a number of assumptions different from those of Team A. Team B assumes the rock body to be impermeable. A very large vertical fracture plane, 800 m X 800 m in size, centered at the wellbore intersection is used. A hydrostatic pressure boundary condition (i.e. sink) is applied at the perimeter of the fracture plane. The fluid viscosity is assumed to be 1 cP for the first four tests, and 10 cP for Test 5. Team B models each of the five test with five separate, independent simulations, implicitly assuming that the pressure/stress perturbation caused by each injection has vanished before the start of the subsequent test.

For Test 5, proppant transport is not explicitly simulated. However, we assumes a "propped" zone, 20 m in radius around the injection point, loosely based on the proppant simulation results of Team A. The fracture aperture in this zone is assumed to be not smaller than 30% of the maximum aperture experienced by the corresponding area during the fluid injection.

The venting/flow-back is not modeled as an instantaneous reversal of flow directions. At the commencement of a venting stage, a pressure boundary condition is applied at the intersection between the fracture and the wellbore, forcing the fluid pressure to linearly decrease from the shut-in pressure to the hydrostatic pressure in five minutes and remain at hydrostatic thereafter.

5.3. Results for Test 1

As the Team B model does not include matrix permeability, and thereby leakoff from the fracture into the matrix, the only mechanism that controls the pressure decline during shut-in is the propagation of the

fluid pressure along the natural fracture. Team B calibrates the Barton-Bandis joint closure model (i.e. the relationship between effective stress and fracture aperture) based on the shut-in pressure decline curve. According to calibrated Barton-Bandis model, the natural fracture has an aperture of 0.08 mm at zero/minimal effective stress and 0.05 mm at an effective stress of 5 MPa. This set of parameters are used for all the simulations by Team B. The simulated shut-in pressure curve is shown in Fig. 6.

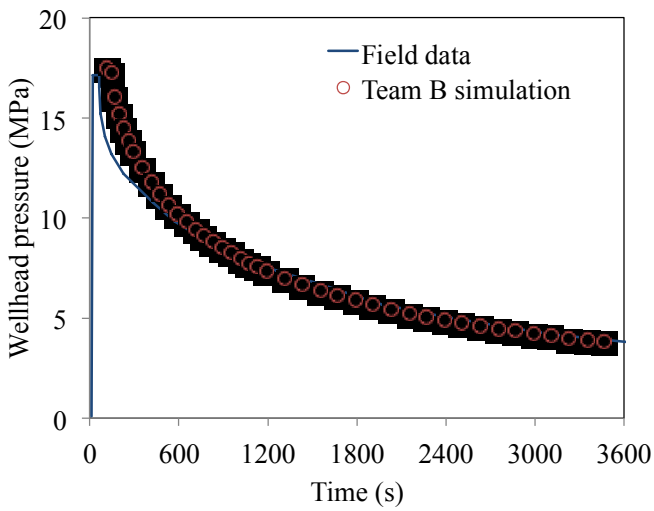

Fig. 6. Simulated Test 1 shut-in pressure decline curve by Team B.

5.4. *Simulation Results for Test 2 and Test 4*

Because Tests 2 to 4 are similar in nature and the injection volume for Test 3 is somewhere between that for Test 2 and Test 4, only Test 2 and Test 4 are simulated.

The aperture field and flow field after 1565 s of injection in Test 2 are shown in Fig. 7. As the vertical gradient of the fracture opening pressure (18.5 MPa/km) is much greater than the hydrostatic gradient (~9.8 MPa/km), the injected fluid has a very strong tendency to migrate upward. During the venting, only the fluid in a relatively small vicinity of the wellbore intersection flows back to the wellbore, whereas the majority of the injected fluid continues to move upward. Additionally, the near-wellbore aperture is very small due to the low effective stress near the wellbore. The simulated wellbore flow rate is shown in Fig. 8. A time integration of the flow rate over the venting period finds that only 3% of the injected fluid flows back.

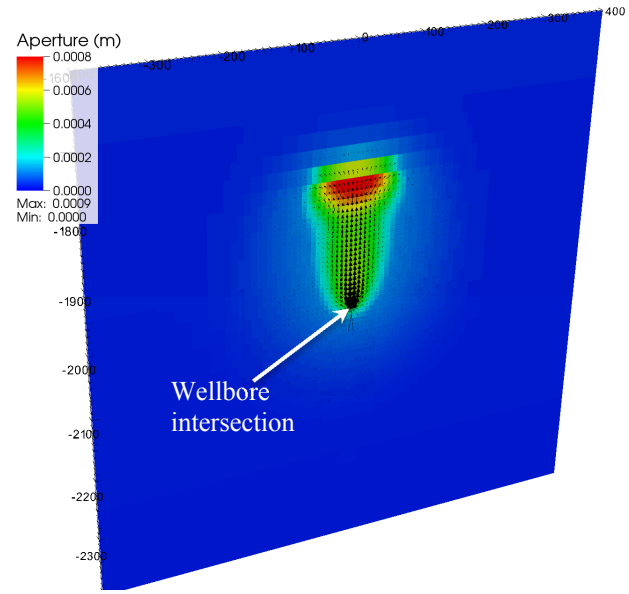

Fig. 7. Aperture distribution after 1565 s of injection in Test 2. The volume of injection at this time is similar to the total injection volume of Test 5. The black arrows denote the direction and rate of flow.

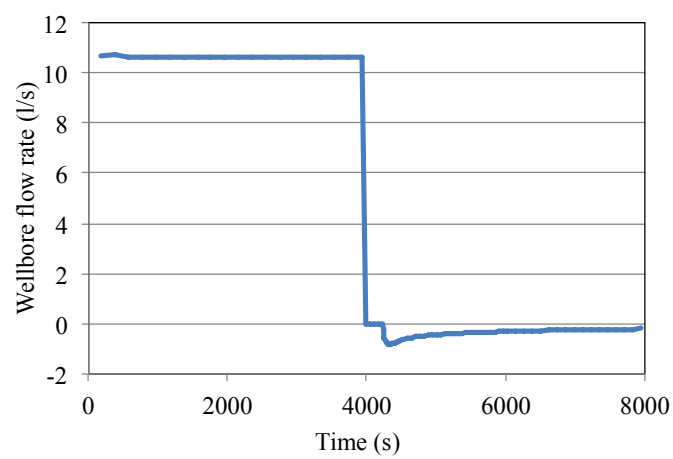

Fig. 8. Simulated wellbore flow rate for Test 2 by Team B. A positive value means injection and negative values mean flow-back.

The simulation results for Test 4 show a very similar pattern: a strong tendency of fluid to migrate upwards and very low flow-back rate. Only 1.3% of the injected fluid flows back during the 1-hour venting. Note that the fluid recovery ratios are comparable to Team A's corresponding results. The remarkable difference in the flow rate at the beginning of the flow back is likely due to the different numerical treatments adopted by the two teams: Team A uses a constant flow-back rate of 5 l/s per fracture until the bottomhole pressure reduces to the hydrostatic pressure and fixed the bottomhole pressure at hydrostatic thereafter; Team B forces a linear transition of the bottomhole pressure from the initial shut-in pressure to the hydrostatic pressure over five minutes.

5.5. *Simulation Results for Test 5*

The dynamic viscosity of the fluid simulated in Test 5 is ten times that for the other four tests. As shown in Fig. 9, high fluid viscosity remarkably impedes the upward tendency of the fluid migration, although the tendency is still discernable. The aperture near the wellbore is larger than 3 mm, also due to the high fluid viscosity. Such a large aperture will allow the proppant to enter the fracture. This also means that the simple propping treatment of Team B results in a near-wellbore residual aperture of approximately 1 mm. The combined effect of these two factors, namely fluid staying near the wellbore and smaller near-wellbore impedance, results in very high (considerably higher than the injection rate) flow-back rate in the beginning of the venting. More than 80% of the injected fluid flows back within one hour according to the simulation.

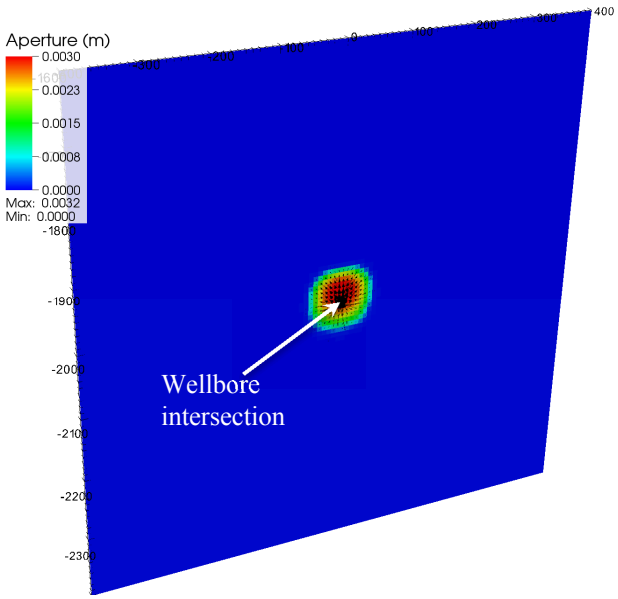

Fig. 9. Aperture distribution at the end of injection (713 s) in Test 5. The total volume of injection is similar to the volume injected in the state of Test 2 shown in Fig. X. Note that the scales of the legend in these two figures are very different.

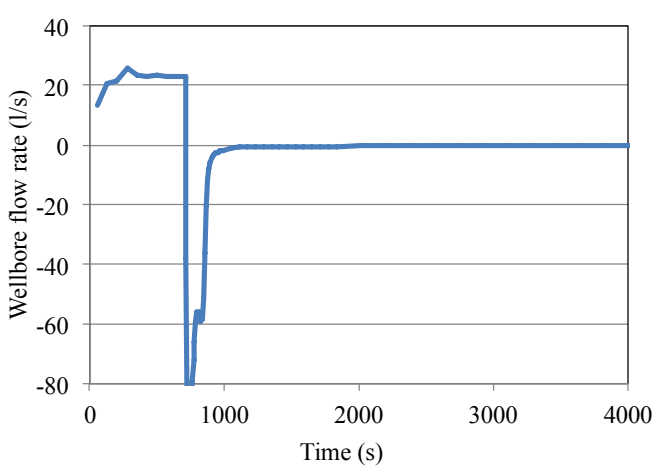

Fig. 10. Simulated wellbore flow rate for Test 5 by Team B. A positive value means injection and negative values mean flow-back.

6. DISCUSSIONS AND CONCLUSIONS

This paper presents a summary of the preliminary simulation results on a series of injection and flow-back experiments at Fenton Hill HDR study, Phase I, from two teams participating in the GTO Code Comparison Study (CCS). Both team assumed that fluid was injected into a pre-existing natural fracture. Despite this similarity, the two teams' models are substantially different from each other in a number of aspects as summarized in Table 2 below. However, both sets of models capture the most important field observations, including the shut-in pressure behavior and the fluid recovery ratios for different injection scenarios quite well. This modeling exercise proves a natural fracture(s) having been opened during the stimulation is plausible to be a plausible hypothesis.

Table 2. Differences between the models by the two teams

	Team A	Team B
Num. method	BEM-FVM	FEM-FVM
Rock permeability	Permeable	Impermeable
Fluid viscosity	1cP for all tests	10 cP for Test 5; 1 cP for others
Relations between tests	As a continuous series	As separate, independent simulations
Natural fracture	170 m X 170 m	400 m X 400 m, sink around perimeter

The simulation results from both teams suggest that low water recovery ratios in Tests 2 to 4 were mainly caused by the great (much greater than the hydrostatic gradient) vertical gradient of the fracture opening pressure. This resulted in a very strong tendency of the injected fluid to migrate upward. When the flow-back started, most of the injected fluid continued to migrate upward, instead of flowing back to the wellbore. Additionally, during flow-back the pressure near the wellbore was much lower than the fracture opening pressure at the depth, inducing high near-wellbore hydraulic impedance. The high fluid recovery ratio in Test 5 was the combined effects of at least three factors: 1) high viscosity impeded fluid's upward migration tendency; 2) relatively small injection volume allowed most of the injection fluid remain near the wellbore; and 3) the injected proppant greatly reduced the near-wellbore hydraulic impedance during flow-back.

In a separate modeling exercise, we investigated the effects of the cooling of the rock surrounding the fracture due to the injection of cold water. We found that the cooling could increase the near-wellbore aperture by 0.7 mm when the fracture is jacked open. This could further aid the entrance of the proppant into the fracture and reduce the flow-back impedance. The results are not included in the present paper.

The available data is limited, and as a result, simulation matches to the data are highly nonunique. Therefore, the simulations should be interpreted as ways of exploring the viability of a particular hypothesis about the process. They do not rule out other interpretations of the data. A key value of the simulations is to develop insight into the system through sensitivity analysis. Sensitivity analysis simulations were performed in the process of generating these matches to the data, but for brevity, they are not summarized here.

The sensitivity analysis indicates that some of the most important factors that control the overall behavior of the system are: the aperture at effective normal stress of zero, the effective stress sensitivity to aperture, the matrix permeability, and the total size of the fracture. Lowering aperture at effective normal stress of zero decreases the rate of pressure decline after the first injection by slowing the rate of fluid spreading in the fracture. Increasing the stress sensitivity to aperture causes greater pinchoff near the well during flowback, reducing fluid recovery. Increasing matrix permeability causes greater leakoff of fluid into the surrounding formation, reducing fluid recovery. Note that the matrix permeability in the simulation (not included in Team B's models) may include not only flow in the intact rock, but also flow in small-scale fractures. Increasing the total size of the fracture enables further spreading of fluid away from the well, reducing fluid recovery.

ACKNOWLEDGMENTS

Support from the US Department of Energy Geothermal Technologies Office is gratefully appreciated. Pengcheng Fu's work was performed under the auspices of the U.S. Department of Energy by Lawrence Livermore National Laboratory under Contract DE-AC52-07NA27344.

REFERENCES

Reference to a journal article:

1. Barton, C., M. D. Zoback, and K. L. Burns. 1988. In-situ stress orientation and magnitude at the Fenton Geothermal Site, New Mexico, determined from wellbore breakouts. *Geophysical Research Letters*, 15(5), 467-470.
2. Barton, N, S. Bandis, and K. Bakhtar. 1985. Strength, deformation and conductivity coupling of rock joints. *Int J Rock Mech Min Sci Geomech Abstr,* 22:121–140.
3. Brown, D. W. 1989. The potential for large errors in the inferred minimum earth stress when using incomplete hydraulic fracturing results. *Int J Rock Mech Min Sci Geomech Abstr,* 26(6): 573-577.
4. Brown, D. W., D. V. Duchane, G. Heiken, and V. T. Hriscu. 2012. Mining the Earth's Heat: Hot Dry Rock Geothermal Energy, Springer-Verlag.
5. Crouch, S.L. and A.M. Starfield. 1983. *Boundary element methods in solid mechanics*. 1st ed. London: George Allen & Unwin.
6. Dontsov, E., and A. Peirce. 2014. Slurry flow, gravitational settling and a proppant transport model for hydraulic fractures. *Journal of Fluid Mechanics*, 760: 567-590.
7. Fourar, M., S. Bories, R. Lenormand, and P. Persoff. 1993. Two-phase flow in smooth and rough fractures: measurements and correlation by porous-medium and pipe-flow models. *Water Resources Research*, 29(11): 3699-3708.
8. Fu, P., S.M. Johnson, and C.R. Carrigan. 2013. An explicitly coupled hydro-geomechanical model for simulating hydraulic fracturing in arbitrary discrete fracture networks. *Int J Numer Anal Methods Geomech*, 37:2278–2300.
9. Hazzard, J.F., R.P. Young, and S.C. Maxwell. 2000. Micromechanical modeling of cracking and failure in brittle rocks. *J. Geophys. Res.* 105: 16,683–16,697.
10. Kelkar, S., H. Murphy, and Z. Dash. 1986. Earth stress measurements in deep granitic rock. Rhe 27th U.S. Symposium on Rock Mechanics, Tuscaloosa, Alabama.
11. McClure, W.M., M. Babazadeh, S. Shiozawa, et al. 2015. Fully Coupled Hydromechanical Simulation of Hydraulic Fracturing in Three-Dimensional Discrete Fracture Networks. Presented at the SPE Hydraulic Fracturing Technology Conference, the Woodlands, TX.
12. McClure, M.W., M. Babazadeh, S. Shiozawa, and J. Huang. 2016. Fully coupled hydromechanical simulation of hydraulic fracturing in 3D discrete-fracture networks, SPE Journal, Preprint, doi:10.2118/173354-PA.
13. Moreland, K. 2014. The ParaView Tutorial, Version 4.2. Sandia National Laboratories.
14. Okada, Y. 1992. Internal deformations due to shear and tensile faults in a half-space. *Bulletin of the Seismological Society of America*, 82 (2): 1018-1040.
15. Settgast, R.R., P. Fu, S.D.C. Walsh, J.A. White, C. Annavarapu, F.J. Ryerson. 2016. A Fully Coupled Method for Massively Parallel Simulation of Hydraulically Driven Fractures in 3-Dimensions. *International Journal for Numerical and Analytical Methods in Geomechanics*, submitted.
16. Shiozawa, S., and M.W. McClure. 2016. Simulation of proppant transport with gravitational settling and fracture closure in a three-dimensional hydraulic fracturing simulator. *Journal of Petroleum Science and Engineering*, 138: 298-314.
17. Vinsome, P. K., and J. Westerveld. 1980. A simple method for predicting cap and base rock heat loses in

thermal reservoir simulators. *Journal of Canadian Petroleum Technology*, 19(3), 87-90.

18. White, M.D., and B.R. Phillips. 2015. Code Comparison Study Fosters Confidence in the Numerical Simulation of Enhanced Geothermal Systems. *40th Workshop on Geothermal Reservoir Engineering*, Stanford University, Stanford, CA.

19. White, M.D., D. Elsworth, E.L. Sonnenthal, P. Fu, and G. Danko. 2016. Challenge Problem Statements for a Code Comparison Study of Enhanced Geothermal Systems. *41st Workshop on Geothermal Reservoir Engineering*, Stanford University, Stanford, CA (2016).